



NURC

a NATO Research Centre
un Centre de Recherche de l'OTAN



PARTNERING
FOR MARITIME
INNOVATION

Reprint Series

NURC-PR-2008-004

Bottom profiling by correlating beam-steered noise sequences

Chris H. Harrison, Martin Siderius

September 2008

Originally published in:

Journal of the Acoustical Society of America, Vol. 123, No. 3, March 2008,
pp. 1282-1296.

Distribution:

For distribution only to NATO, Government Agencies of NATO member nations
and their contractors. No secondary distribution authorized.

About NURC

Our vision

- To conduct maritime research and develop products in support of NATO's maritime operational and transformational requirements.
- To be the first port of call for NATO's maritime research needs through our own expertise, particularly in the undersea domain, and that of our many partners in research and technology.

One of three research and technology organisations in NATO, NURC conducts maritime research in support of NATO's operational and transformation requirements. Reporting to the Supreme Allied Commander, Transformation and under the guidance of the NATO Conference of National Armaments Directors and the NATO Military Committee, our focus is on the undersea domain and on solutions to maritime security problems.

The Scientific Committee of National Representatives, membership of which is open to all NATO nations, provides scientific guidance to NURC and the Supreme Allied Commander Transformation.

NURC is funded through NATO common funds and respond explicitly to NATO's common requirements. Our plans and operations are extensively and regularly reviewed by outside bodies including peer review of the science and technology, independent national expert oversight, review of proposed deliverables by military user authorities, and independent business process certification.



Copyright © Acoustical Society of America, 2008.

NOTE: The NURC Reprint series reprints papers and articles published by NURC authors in the open literature as an effort to widely disseminate NURC products. Users should cite the original article where possible.

Bottom profiling by correlating beam-steered noise sequences

Chris H. Harrison^{a)}

NURC, Viale San Bartolomeo, 400, 19126 La Spezia, Italy

Martin Siderius^{b)}

HLS Research Inc., 3366 North Torrey Pines Court, La Jolla, California 92037, USA

(Received 24 April 2007; revised 30 November 2007; accepted 18 December 2007)

It has already been established that by cross-correlating ambient noise time series received on the upward and downward steered beams of a drifting vertical array one can obtain a subbottom layer profile. Strictly, the time differential of the cross correlation is the impulse response of the seabed. Here it is shown theoretically and by simulation that completely uncorrelated surface noise results in a layer profile with predictable amplitudes proportional to those of an equivalent echo sounder at the same depth as the array. The phenomenon is simulated by representing the sound sources as multiple random time sequences emitted from random locations in a horizontal plane above a vertical array and then accounting for the travel times of the direct and bottom reflected paths. A well-defined correlation spike is seen at the depth corresponding to the bottom reflection despite the fact that the sound sources contain no structure whatsoever. The effects of using simultaneously steered upward and downward conical beams with a tilted or faceted seabed and multiple layers are also investigated by simulation. Experimental profiles are obtained using two different vertical arrays in smooth and rough bottom sites in the Mediterranean. Correlation peak amplitudes follow the theory and simulations closely. © 2008 Acoustical Society of America.

[DOI: 10.1121/1.2835416]

PACS number(s): 43.30.Pc, 43.30.Ma, 43.30.Nb, 43.30.Re [DRD]

I. INTRODUCTION

Ocean noise, or just noise in general, can be viewed in many ways. Traditionally, ocean noise is treated as a nuisance, distinguished only by having a spectrum, directionality, and related properties such as spatial and temporal coherence (Urlick, 1975). It may also be regarded as chaotic with a prediction horizon confined to a few samples (Frison *et al.*, 1996). Alternatively, one may view ambient sound sources as a complex issue in itself. Experimental work has been done on breaking wave statistics (Ding and Farmer, 1994), and on the influence of white caps in noise production (Cato, 2000) and their spatial and temporal distribution (Melville and Matusov, 2002), and detailed statistical models of breaking wave noise have been built (Finette and Heitmeyer, 1996).

This paper concentrates on using the more broad band, featureless wind noise as a tool to infer something about geoaoustic properties rather than about the noise itself or its sources. Buckingham and Jones (1987) were able to extract the seabed's critical angle from vertical coherence measurements. Recent developments in underwater acoustics suggest that the noise may contain substantially more detailed information than one would think. From the noise (power) directionality alone measured with a vertical array it is possible to determine the seabed's reflection coefficient as a function of angle and frequency (Harrison and Simons, 2002), and with

a drifting array one can obtain a (relative depth) subbottom profile (Harrison, 2004). The latter method, which relies on spectral factorization, was explored further by Harrison (2005). One can make use of the spatial coherence of the noise by cross correlating the time series from separated hydrophones to obtain the Green's function from one hydrophone to the other (Roux and Kuperman, 2004). Theory was treated by Roux *et al.* (2005), and the time required for the cross correlation to converge was treated by Sabra *et al.* (2005). Sabra *et al.* (2004) proposed array element localization as an application. Siderius *et al.* (2006) extended this approach to the domain of subbottom profiling by cross correlating the up- and downsteered beam time series from a drifting vertical array. The aim of the current paper is to develop a quantitative formula for the steered beam correlation amplitude in terms of depth, reflection properties, bandwidth, and so on, and to check it by simulation and by reference to experimental results.

To provide a clear demonstration that no special surface coherence properties are required, all the physical noise mechanisms are deliberately stripped out, and the physics is generalized by postulating an environment with many point sources distributed randomly, but uniformly in a horizontal plane, all emitting random time sequences uniformly in angle (disregarding any surface interference effects). Beneath this is a directional receiver, and beneath that a reflecting seabed as shown in Fig. 1. The aim is then to demonstrate the quantitative behavior of the normalized cross correlation $C(\tau)$ between two steered beam time series g_1, g_2 ,

^{a)}Electronic mail: harrison@nurc.nato.int.

^{b)}Electronic mail: siderius@hlsresearch.c

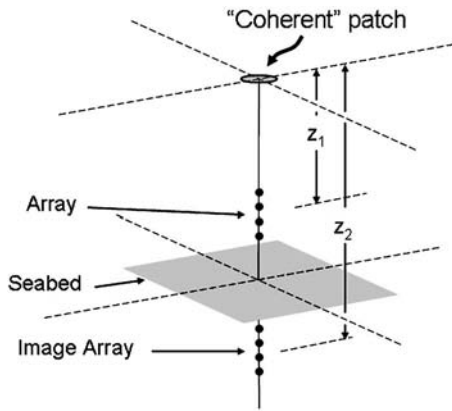


FIG. 1. General geometry showing a coherent patch of noise sources on the sea surface with the actual vertical array and its image reflected in the seabed.

$$C(\tau) = \frac{\int g_1(t)g_2(t + \tau)dt}{\sqrt{\int g_1^2(t)dt \int g_2^2(t)dt}} \quad (1)$$

by estimating the numerator (i.e., the unnormalized cross correlation) and the denominator (i.e., the standard deviations) separately. The values near, and away from, a correlation peak are derived in the Appendix, treating the receiver as a point from which emanates an upward and a downward beam. This yields formulas, which are summarized in Sec. II, in terms of sample rate, bandwidth, and array size.

It is stressed that although the normalization in Eq. (1) seems like a fairly obvious choice, it is by no means the only choice. If, for instance, the g_2 in the denominator were swapped for g_1 the result would be a quantity rather close to a time domain representation of $\overline{g_1(\omega)g_2(\omega)}/|g_1(\omega)|^2$, which is a coherent version of the ratio of the downward to upward beam spectral powers, i.e., $|g_2(\omega)/g_1(\omega)|^2$, as used to determine reflection coefficient by Harrison and Simons (2002). This suggests that in the time domain alternative normalizations could be used to determine, for instance, absolute reflection coefficients, though this will not be pursued here.

In Sec. III the same calculation is approached as a simulation, retaining the processing algorithms already used on experimental data (Siderius *et al.*, 2006). Noise files are simulated for each hydrophone of a vertical array using random number sequences added and shifted in time according to their position relative to the array. The latter approach underscores the “emergent” property of the correlation, since the sources’ sequences are entirely incoherent and do not contain any identifiable “clicks” or “splashes.” This approach is used to investigate processing techniques, the effect of seabed reflection coherence, bottom tilt, and angle resolution of individual scatterers.

Finally in Sec. IV these findings are applied to experimental data from three vertical array drift experiments in the Mediterranean, two over smooth seabed and two over rough.

II. THEORY

The relationship between the time derivative of the noise correlation function and the time domain Green’s functions between hydrophones is well established (Weaver and

Lobkis, 2004; Roux *et al.*, 2005) and it is not the main interest here. Instead the paper attempts to construct and justify a function, or functions, and their normalizations that predict something useful about the seabed other than travel times.

A. Peak amplitude formula

In the Appendix it is shown that the numerator (actually peak value) of Eq. (1) can be expressed in terms of the depths of the receiver and its image in the seabed z_1, z_2 , the autocorrelation function of the sound sources $C_s(\tau)$, the speed of sound c , and a constant K_0 as [Eq. (A10)]

$$\int g_1(t)g_2(t + \tau)dt = K_0 \frac{c}{(z_2 - z_1)} \int_{\tau - z_2}^{\infty} C_s(\tau')d\tau'. \quad (2)$$

The peak value of the time differential of this quantity is derived through the discrete difference Δ operator, the sample frequency f_s , and the reflection coefficient $R(\theta)$ as [Eq. (A14)]

$$\max \left[\Delta \left\{ \int g_1(t)g_2(t + \tau)dt \right\} \right] = K_0 R(0) \frac{c}{f_s(z_2 - z_1)}, \quad (3)$$

where “max” means the maximum of the absolute value multiplied by sign, remembering that the impulse could be negative. The denominator of Eq. (1) can be expressed in terms of the same constant K_0 , the number of hydrophones M , a numerical constant β dependent on noise coherence and shading, as [Eq. (A22)]

$$\sqrt{\int g_1^2(t)dt \int g_2^2(t)dt} = K_0 |R(0)| \frac{\beta}{M}. \quad (4)$$

So the final peak value of the cross correlation is [Eq. (A25)]

$$\max[\Delta\{C(\tau)\}] = \frac{2L \text{sign}(R)}{(z_2 - z_1)\gamma\beta}, \quad (5)$$

where L is the array length and γ is the ratio of sample frequency to design frequency for the array: $\gamma = f_s/f_0$.

The main dependence of the peak correlation height is on array length and its separation from the seabed. Although the peak depends on the sign of the reflection coefficient it does not depend on the reflection strength. A simple explanation for this can be seen through the three areas shown in Fig. 2. The numerator of Eq. (1) depends on noise received in the small area in which the times of arrival differ by a few samples ($\sim 1/f_s$). Applying the Fresnel approximation to the geometry shown in Fig. 1 one can see that this area is of order $2\pi(c/f_s)z_1z_2/(z_2 - z_1)$. In contrast, the denominator of Eq. (1) depends on noise received in the larger areas illuminated by the upward and downward endfire beams. Since the endfire beam width is roughly $\sqrt{2/M}$, these areas are, respectively, $2\pi z_1^2/M$ and $2\pi z_2^2/M$, and their geometric mean is $2\pi z_1z_2/M$. The order of magnitude peak value depends on the ratio of the small area to this geometric mean area, i.e., $Mc/\{f_s(z_2 - z_1)\}$, and this clearly reduces to the quantity evaluated in Eq. (5).

As estimated in the fourth section of the Appendix, for a 32-element array 30 m above the seabed with 12 kHz sam-

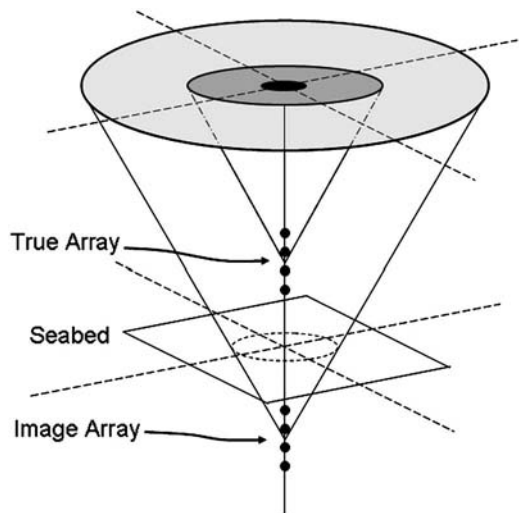


FIG. 2. The three important areas of noise sources on which the normalized cross correlation depends. The numerator of Eq. (1) depends on the small coherent area; the upbeam and downbeam parts of the denominator (standard deviations) depend, respectively, on the intermediate and largest areas.

pling, 4166.7 Hz design frequency (0.18 m hydrophone spacing), and minimal filtering, a peak height of ~ 0.016 is expected.

Interestingly, because of the normalization, the magnitude does not depend on the reflection coefficient R or frequency band particularly. However it will be seen in Sec. IV that there are geographic variations of “echo” strength in the experimental data. So an explanation will be sought. An important point is that the correlation peak as estimated here is an “emergent” property (see, e.g., Sabra *et al.*, 2005) that does not depend on any source coherence, i.e., clicks or splashes.

The above-presented explanations and the derivation in the Appendix assume the noise to have a flat frequency response. It is shown in the Appendix that as long as the near zero frequencies are excluded there is another processing option using a Hilbert transform with, or without, the time differentiation. The price paid for this more robust solution is loss of information on sign of the reflection, which translates to an inability to distinguish between increase and decrease of acoustic impedance.

Generally, if one is only interested in the timing of the layering rather than its exact impulse response there are more options. Since taking the time derivative is equivalent to multiplying by frequency in the frequency domain, and the noise has its own initial spectrum, there is some freedom in the prefiltering of the signal and in postfiltering the time-domain correlation function. According to Weaver and Lobkis (2004) “the spectral power density of the diffuse field may be thought of as a filter and the source of some distortion between the time derivative of the Green’s function and the field-field correlation function.” Indeed it is straightforward to demonstrate numerically that, for instance, multiplying the cross spectral density by frequency (postfiltering) is identical to multiplying the two initial noise signals by the square root of frequency (prefiltering). Thus no generality is lost in the definition, Eq. (1), if the time series of the up- and downsteered beams $[g(t)]$ are allowed already to be filtered.

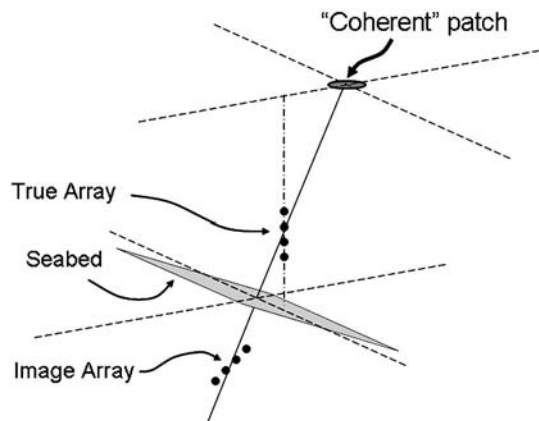


FIG. 3. Geometry equivalent to that in Fig. 2 but for a tilted seabed, showing the tilt of the array image and the horizontal offset of the coherent patch.

Furthermore, in these authors’ experience one can obtain depth-accurate subbottom layer profiles from noise correlation without worrying about detailed filtering as long as the lowest frequencies are extracted, but more care needs to be taken to obtain other properties such as reflection coherence.

B. Criterion for detecting a bottom “echo” in uncorrelated background

Away from the correlation peak value there is a decorrelated background, and it is shown in the Appendix that, if the number of independent samples in the cross correlation is N_s , then the background level for the normalized cross-correlation function [Eq. (1)] is $N_s^{-1/2}$. Thus the criterion for detecting a sediment layer or “echo” is that the quantity in Eq. (5) must be greater than $N_s^{-1/2}$, preferably a lot greater. To detect the peak height estimated in Sec. II A (0.016) one needs about 4000 independent samples. Conversely a 10 s random time series sampled at 12 kHz results in a background level of $(120\,000)^{-1/2} = 0.0029$, i.e., about one-fifth of the peak value. Of course, in practice to obtain a useful impulse response containing many peaks, one requires the background to be below the weakest peak, so ultimately there is a constraint on the number of samples required and the relative motion of the receiver and target.

C. Additional layers

The addition of a layer is a trivial extension to the theory. It can be seen that the standard deviation of the noise (denominator) responds to the combined reflected power from all the layers whereas the peak value only responds to the layer at the delay of the peak in question. Therefore the cross correlation is a proportional representation of the seabed’s impulse response; the layer echoes scale in the same way as with an echo sounder, and they retain their signs.

D. Bottom tilt, tilted facets

In order to see the effects of reflecting facets a tilted plane seabed is considered first. The geometry in Fig. 3 shows that there are still three areas determining the normalized cross correlation. The small coherent area is centered on the point where the projection of the line joining the receiver

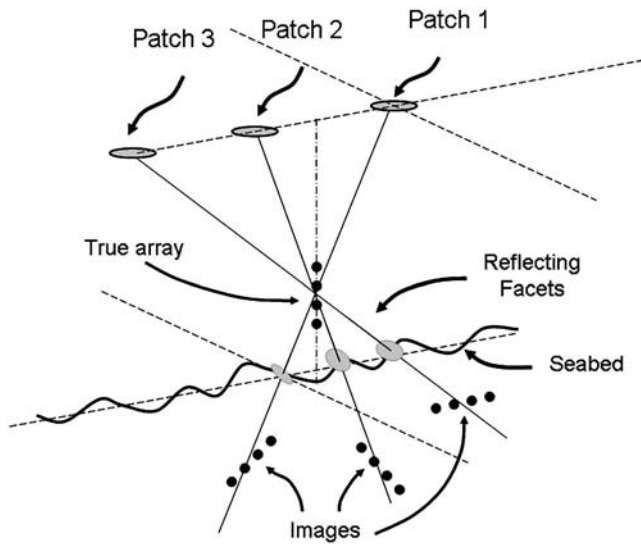


FIG. 4. Images and coherent areas for a rough faceted surface with multiple specular reflections. The three example facets each have their own corresponding tilted image array and coherent patch.

and its image meets the sea surface. However it can only contribute if the upward and downward beams are steered appropriately. For example, with a bottom slope α this coherent patch appears in the center of the upward beam steered to α (from vertical). The image array is tilted at 2α to the vertical, as shown in Fig. 3, so the coherent area appears in the center of the image array's beam (also steered at α from the vertical). It is therefore appropriate to use the same steer angle for the upward and downward beams. The incoherent areas contributing to the denominator of Eq. (1) then depend on the steer angles, but despite quite complicated geometry, the dependence is weak. In the case of a rough surface composed of facets with a distinct Fermat extremum path as in Fig. 4, the above-mentioned reasoning can be applied to each facet. Thus one expects a correlation peak for each correctly (i.e., specularly) oriented facet. One also expects the peak to be resolvable in steer angle given adequate array aperture.

E. Bottom reflection coherence

The analysis in the Appendix assumes that the reflecting layer is perfectly flat. It also assumes that the bottom structure does not change during the collection of the samples to be correlated. In one of the experimental examples of sec. IV it is suspected that neither of these assumptions is true. In principle, given a rough surface, stationary geometry, and unlimited time, one might still expect performance comparable with an echo sounder even though the reflector is not specular. According to the Rayleigh criterion (Brekhovskikh and Lysanov, 1982) if the vertical roughness scale is greater than $\lambda/4\pi$ the surface behaves like many reflecting facets as seen in Fig. 4. By itself this simply spreads the energy of the single peak (expected for a specular reflector) amongst several others. Thus the echo is smeared in time. If the receiver is moving, these nonvertical arrivals shift in travel time and therefore blur. By considering a tilted specular reflector one can see that when the roughness scale is very large the

motion-blurring effect is quite distinct from the roughness-smearing since it depends on drift speed. Rather than attempt to explain these effects quantitatively they are demonstrated by simulation in Sec. III.

F. Sound source coherence

So far it has been assumed that the sound sources are completely incoherent. Here the effect of significant source coherence is considered. Imagine a single impulsive source at the sea surface with no other background. The normalized cross correlation will have peak value unity [i.e., much greater than predicted by Eq. (5)], since it is normalized. Therefore it is conceivable that from time to time, or in particular weather states, there can be another more obvious, and nonemergent, correlation mechanism. This is not investigated further but it will be borne in mind in Sec. IV.

III. SIMULATION

A. Data generation

Having established formulas for peak height and background the cross correlation is now investigated by simulation. The approach here differs from earlier simulations (e.g., Siderius *et al.* (2006)) in placing more emphasis on the randomness of the sources than on ducted propagation. The geometry of the array and sources is as in Fig. 1, but the orientation of the seabed will vary from case to case. The sea surface sources are spread uniformly but randomly within a circular area centered on the extrapolated line through the receiver and its image (see Figs. 1 or 3, as appropriate). From each point emanates a unit variance, Gaussianly distributed random sequence of 131 072 ($=2^{17}$) samples. Each sequence is assumed to be sampled at 12 kHz and to propagate from this surface point to each of the hydrophones on the array and their images. The time series are delayed according to geometry by phase shifting in the frequency domain. The 32-element array has hydrophone separation 0.18 m (design frequency 4167 Hz) and is centered at depth 50 m in 80 m of water. It is well known that the sum of power contributions from monopole sources on an infinite flat surface does not converge (Harrison, 1996) unless there is some loss mechanism. In this simulation, partly for this reason and partly for the sake of realism, dipole sources are assumed, and otherwise convergence is ensured by relying on the steered beam directionality. Unless otherwise stated the radius of the circular area of sources is 150 m. The end result is a file containing 32 time series approximately 11 s long, one for each hydrophone. To study the effects of coherently or incoherently adding the correlation functions, the whole process was repeated with new random number seeds to form 81 files.

B. Data processing

Data processing for the simulated time sequences is identical to that already used for experimental data. Generally the time series for each hydrophone is filtered, then it is time-domain beam-formed with hamming shading, and finally cross correlated in the frequency domain, and differenced to form a finite difference time differential. If the time

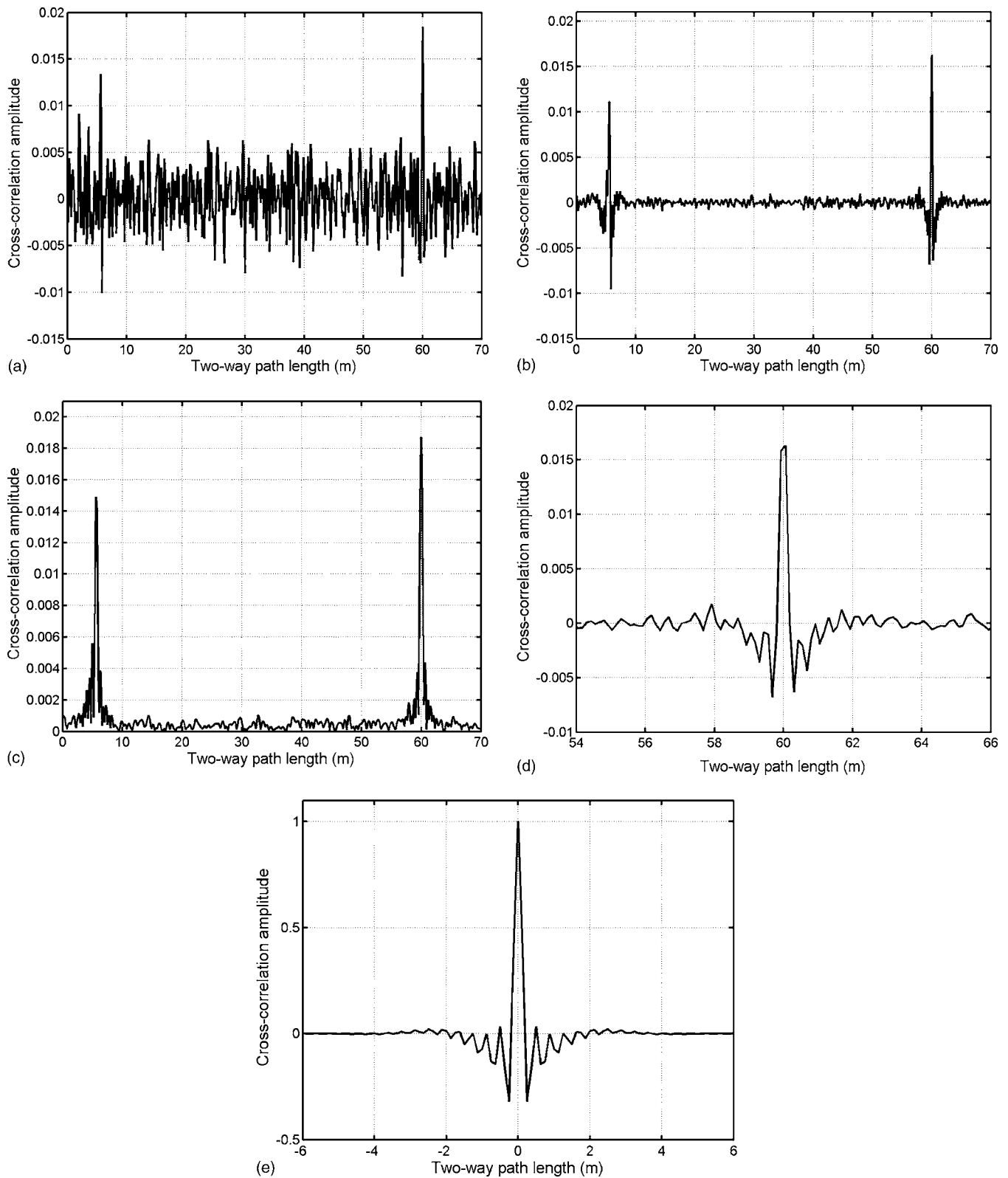


FIG. 5. Simulation of the cross correlation resulting from (a) a single 11 s file showing a peak at two-way travel time corresponding to 60 m, (b) 81 coherently added 11 s files, (c) the Hilbert transform corresponding to 81 files, (d) a blow-up of the peak in (b), and (e) the impulse response of the initial bandpass filter.

series is to be Hilbert transformed then the initial filter is used to exclude the near zero frequencies. Since the spectrum of the simulated sources is already flat there is no need to normalize the spectrum, but it is important to cut out frequencies close to and above the design frequency. For this reason a bandpass filter between 400 and 3900 Hz was used.

C. Test cases

1. Horizontal plane reflector

Figure 5(a) shows the time differential of the cross correlation between the “up” and “down” vertical beams evaluated according to Eqs. (1)–(5) for a single file (lasting 11 s).

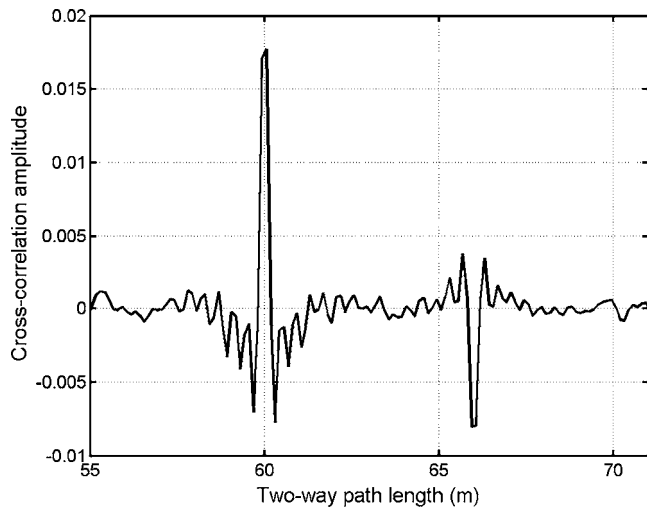


FIG. 6. Simulation of the cross correlation resulting from two layers, one at 30 m below array center with a reflection coefficient of 0.1, the other at depth 33 m with a reflection coefficient of -0.05 .

Figure 5(b) shows the reduction in the background on coherently adding 81 files (approximately 15 min), and Fig. 5(c) shows its Hilbert transform. In both cases the peak is at a delay corresponding to 60 m (i.e., $z_2 - z_1$) and its height is approximately the same in both cases ~ 0.018 , which agrees closely with the earlier estimate in Sec. II A and is independent of the assumed reflection coefficient which was 0.1. At much shorter range (5.7 m) there is apparently another peak. This is an artifact that corresponds to the physical length of the array, as can be verified by removing or altering the beam shading.

The standard deviations of the background levels in Figs. 5(a) and 5(b) are, respectively, 0.0029 and 0.000325. Their ratio (≈ 8.9) clearly follows the $N^{1/2}$ prediction of $\sqrt{81} = 9$. Low-pass filtering at 3.9 kHz of a signal sampled at 12 kHz broadens the autocorrelation peak to approximately three samples, so the number of independent samples in a single file is $131\,072/3$ and the absolute background level $N^{-1/2}$ is 0.0048, which agrees well with Fig. 5(a).

A blow-up of the peak arrival shape is shown in Fig. 5(d), and this can be seen to be almost identical to the impulse response of the initial bandpass filter [Fig. 5(e)], as one would expect.

2. Additional plane reflector

A second layer at sediment depth 5 m with reflection coefficient -0.05 is simulated by adding the appropriately delayed source sequences to the existing layer response. No attempt is made to account for multiple reflections in this demonstration. Adding 81 files coherently two impulses can be seen in Fig. 6, the first corresponding to the reflector at depth 80 m (round-trip path length 60 m) with $R=0.1$, the other corresponding to the second reflector at depth 83 m (round-trip path length 66 m) with $R=-0.05$. Clearly the delays and the relative peak amplitudes, including the sign, are correctly reproduced.

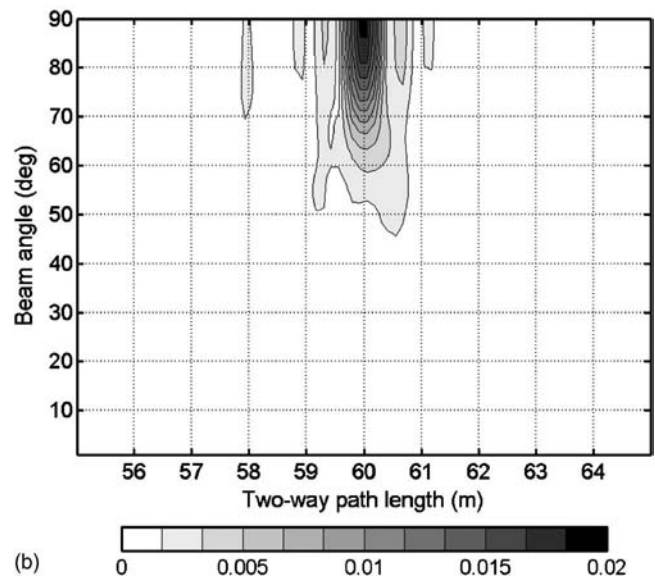
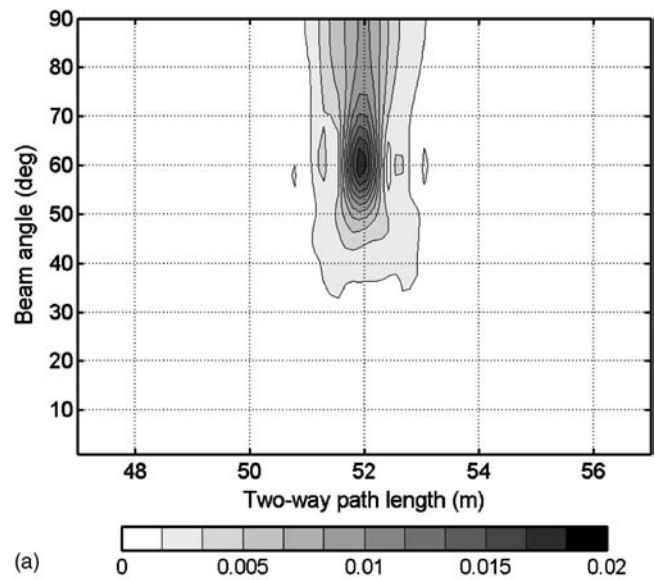


FIG. 7. Correlation amplitude against round-trip path length and steered beam angle for (a) seabed tilted at 30° and (b) horizontal seabed.

3. Tilted plane reflector

To make the point, a large tilt angle of 30° is assumed, so the image array is displaced as shown in Fig. 3, and the area of sources is centered on the small coherent area which is similarly displaced. The result is dependent on steer angle as well as delay and is shown in Fig. 7(a). Since the water depth at the array location is still 80 m the path length to the peak is $2 \times 30 \times \cos(30) = 51.9$ m. The peak in Fig. 7(a) agrees with this delay, and also it is centered on a steer angle of 60° . It is instructive to compare this with the corresponding plot for the horizontal seabed Fig. 7(b). This shows a peak at the obvious delay and angle. In these examples angle resolution is relatively poor because the simulation is of an existing realistic system. However there are no restrictions on improving the resolution by increasing the number of hydrophones. According to Eq. (5) (which, of course, already includes array gain effects) this will also increase the peak height.

One might consider extending simulation to a point target. Interestingly, this requires no extra work since the results would differ from the tilted plane reflector only by a time shift and a calculable change in amplitude. Suppose the plane reflector is removed and the image receiver is replaced with a point target. The downbeam path then goes from source to target to receiver, and the upbeam path is unchanged. All that has changed is the addition of a constant delay between the target and the receiver. Thus a point target in this orientation would appear as the peak in Fig. 7(a) but with amplitude according to its target strength. There is, in fact, strong experimental evidence in the second and third examples of Sec. IV that targets can be detected by this method. Note that it is the particular normalization of Eq. (5) that makes the bottom peak height independent of the seabed reflection coefficient. Other reflectors or scatterers will be reduced in proportion.

4. Rough reflector

In principle it would be possible to extend the current numerical simulation to a rough surface by exchanging the downward specularly reflected path for the many paths connecting each sound source with each hydrophone via a large number of scattering facets [for instance, using the Kirchhoff approximation (Brekhovskikh and Lysanov, 1982)]. Because of the large computation time a simpler approach is preferred, since in this context the only interest is in the effect of decorrelation on peak height. For similar reasons horizontal motion of the array is neglected. According to the Rayleigh criterion the coherence is affected only by the vertical scale of the roughness compared with the wavelength. So a crude way to model this is to add a zero-mean, Gaussianly distributed distance with variance σ^2 to the path difference for each sound source. Because the sources are bandpass filtered with the low pass at 3900 Hz the limiting “roughness” is expected to be $c/(4\pi 3900) = 0.18/(2\pi) \sim 0.03$ m. A set of roughnesses σ was chosen between 0 and 0.5 m, and 81 files generated for each. Selecting a single file for each roughness it is difficult to see much dependence on σ because the sample length is not long enough for convergence. The effect is clearer after coherent integration over the 81 files. The change in peak amplitude is plotted against σ in Fig. 8; the symbols indicate amplitude with, and without, Hilbert transformation. The main effect of the roughness in the time domain is a time smearing, so one might expect smearing proportional to the roughness and peak height proportional to the peak width or some power of it. Superimposed on the plot is an exponential fit and a power law fit. These have no significance other than to reinforce the fact that the peak height is more or less inversely proportional to the roughness (as modeled here).

IV. EXPERIMENTAL DATA

Three experiments have been carried out in the Mediterranean using a drifting vertical array (see Fig. 9). The first two started from more or less the same place on the Malta Plateau, a smooth layered sediment seabed, south of Sicily (Site 1). In April 2002 32 elements at 0.5 m separation (de-

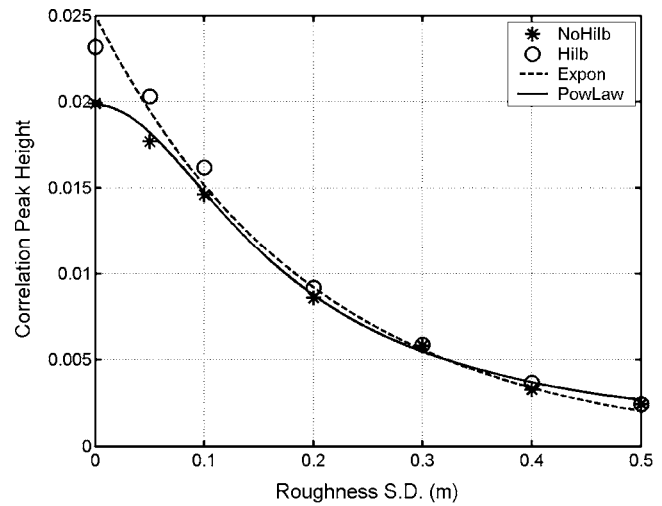


FIG. 8. Plot of correlation peak heights against roughness parameter σ with (O) and without (*) Hilbert transform. Two possible line fits are shown.

sign frequency 1500 Hz) were taken from the center portion of a 62 m nested vertical array (VLA), and a drift of 11 h resulted in a 9 km track. In July 2003 a medium frequency array (MFA) with 32 elements spaced at 0.18 m (design frequency 4167 Hz) drifted for 13 h resulting in a 6.5 km track. In May 2004 the second array drifted on two occasions (12 and 13 May) over parts of the Ragusa Ridge, a very rough rocky area with two main ridges and many sediment filled pools. The first drift covered 5 km in 10 h; the second covered 14 km in 14 h. As ground truth, seismic boomer layer profiles are available near the 2002 drift, and as accurately as possible, exactly along the 2003 drift track. A chirp sonar is available along the 2004 drifts, however it shows little, if any, bottom penetration. Better detail of the bottom roughness is shown by side-scan sonar. The noise data collected in

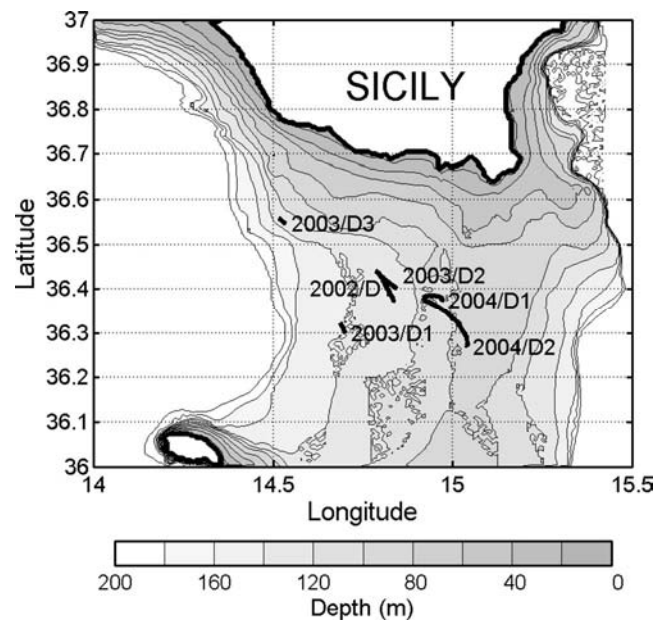


FIG. 9. Map showing the three drift experiments. The 2002 track using a 62 m VLA on the Malta Plateau is labeled 2002/D. The 2003 track using a 6 m MFA on the Malta Plateau is labeled 2003/D2. The two tracks using the MFA on the Ragusa Ridge are labeled 2004/D1 and 2004/D2.

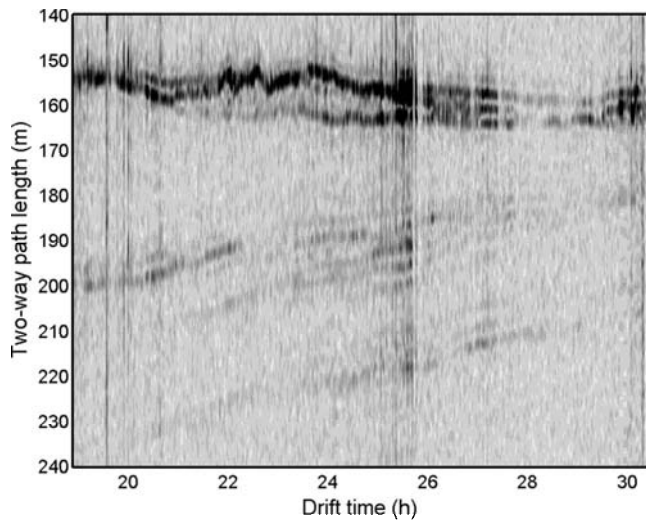


FIG. 10. Subbottom profile from drifting VLA on the Malta Plateau (2002) showing deep echoes.

2002 have been reported in the context of a different processing technique (Harrison, 2004); the 2003 data were also discussed in that context (Harrison, 2005) and in the context of cross-correlation techniques (Siderius *et al.*, 2006). Favorable comparisons have already been made between noise inversion techniques and the various ground truths.

A. Malta Plateau 2002

Each file is approximately 11 s long (65 536 samples at a sampling rate of 6 kHz) so there is the freedom to analyze file by file or to concatenate contiguous files (or equivalently add the processed results coherently) or to smooth the resulting profile. Here it is chosen to analyze file by file and then to process in various ways. Figure 10 shows a profile where a postprocess horizontal smoothing has been applied (incoherent over about 10 files). The seabed is seen at a two-way path length of about 160 m from array center. As well as strong layering in the first 5 m (10 m two-way path as shown) there are clear indications of deep layers at 25 and even 40 m (i.e., 50 or 80 m longer path than the seabed's). Bearing in mind that these calculated depths are simply travel times converted with sound speed in water (assumed 1500 m/s) the actual layer depths are likely to be somewhat greater.

A typical Hilbert transformed correlation amplitude showing a strong, deep second layer echo (at drift time 19:12:00) is shown in Fig. 11(a). A blow-up of the main peak with Hilbert envelope is shown in Fig. 11(b). Another example from 27:00:00 shows a triple echo (see Fig. 10) and its Hilbert envelope. Because the processing used a narrower band (half the design frequency) than the simulated example in Fig. 5 the impulse response is slightly oscillatory, but even so, in Fig. 11(c) it is possible to see differences in phase or sign in the three echoes.

The peak amplitude (averaged over 100 files) is slightly variable throughout the drift (Fig. 12) with a mean between about 0.02 and 0.03. The expected value from Eq. (5) with $\gamma=6000/1500$, $\beta=1.87$ (bandwidth is half the design frequency), $z_2-z_1=150$ m is 0.0285, and this agrees well with

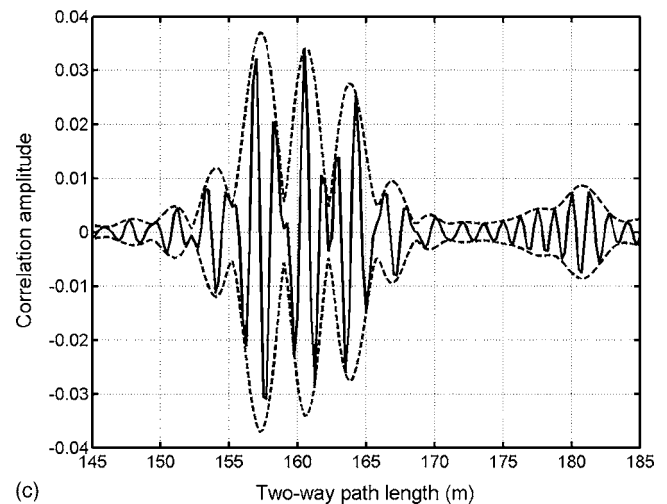
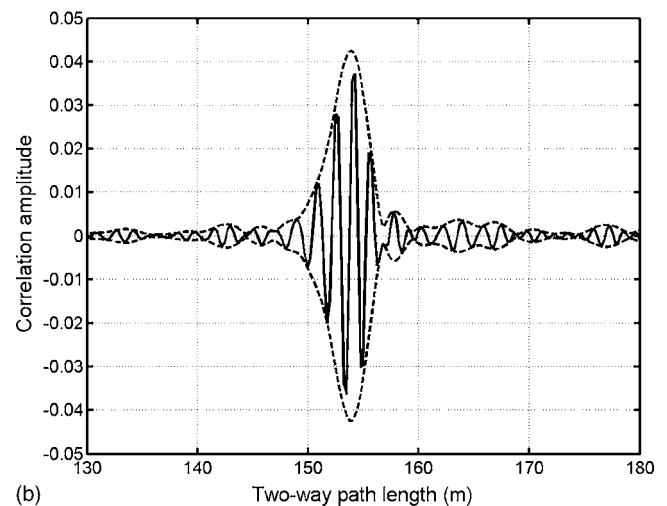
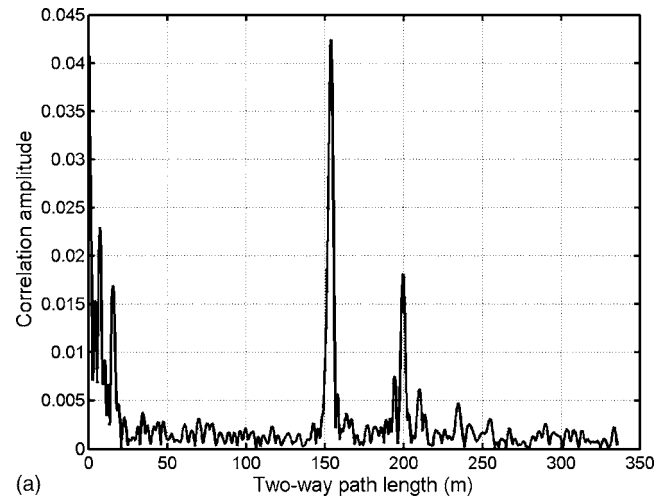


FIG. 11. (a) Hilbert transformed impulse response (average of 100 files) during the 2002 drift (time 19:12:00), (b) blow-up of the main peak showing correlation amplitude with Hilbert envelope, and (c) a triple echo with Hilbert envelope (27:00:00).

the experimental mean. One might expect a slight upward bias of the experimental data in this kind of presentation because the weak peaks are never seen since they are swamped by the background. The variation, in itself, is no surprise and could in principle be averaged out with a stationary array. It is conceivable that from time to time an

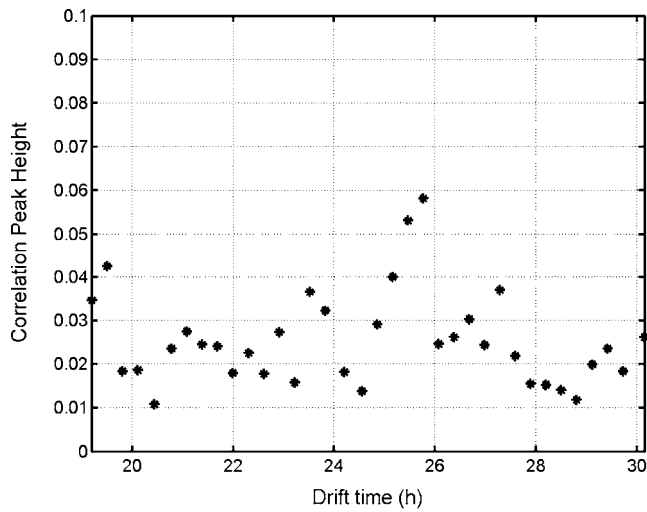


FIG. 12. Correlation peak amplitude (averaged over 100 files) vs drift time during the 2002 drift with the VLA.

exceptionally coherent “clap” from an individual wave might deviate strongly from the normal background “hiss” of wind noise. From the nature of Eq. (1) it is clear that correlation peak heights increasing right up to one are mathematically allowed; they are just extremely unlikely with wind sources.

B. Malta Plateau 2003

Figure 13 shows the profile resulting from the drift of the MFA in 2003. Detailed comparisons have already been made with the profile generated by a seismic boomer subsequently towed along the same track (Siderius *et al.*, 2006). Again two-way paths of 50 m, indicate layer depths of at least 25 m.

A typical Hilbert transformed correlation amplitude (averaged over 100 files around 23:00:00) is shown in Fig. 14(a). Each file is approximately 10 s long (122 880 kHz samples at a sampling rate of 12 kHz). The double peak with Hilbert envelope is blown up in Fig. 14(b). Although the design frequency is now 4167 Hz the relative band is the same as in the VLA case and so the impulse response has the

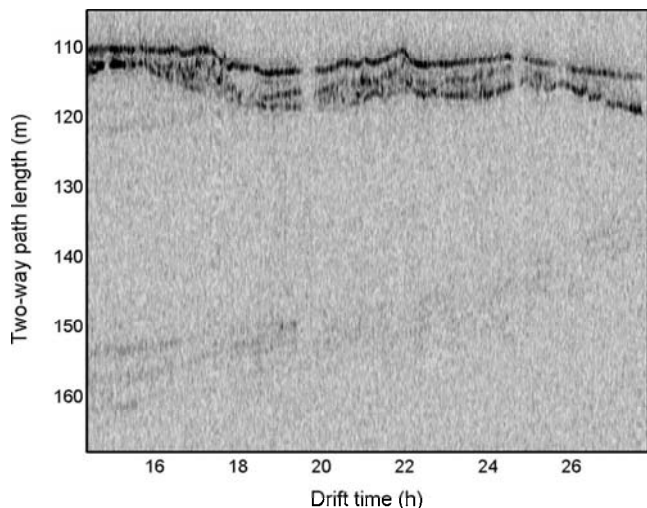


FIG. 13. Subbottom profile from drifting MFA on the Malta Plateau (2003) showing deep echoes.

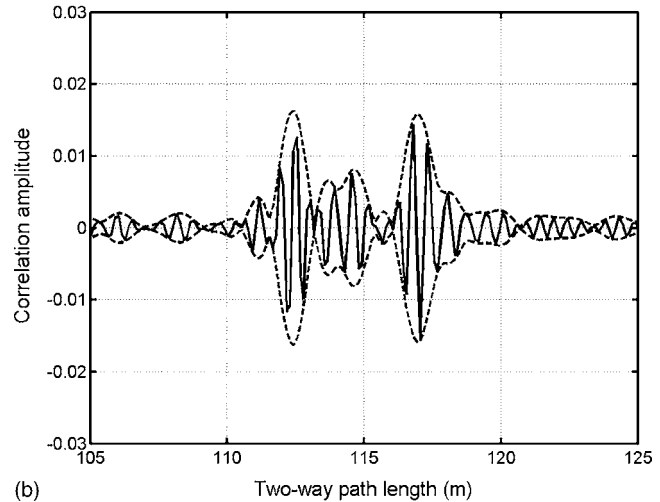
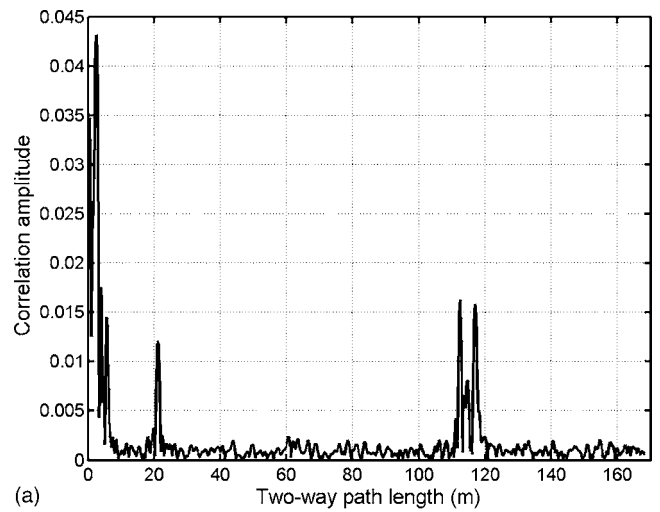


FIG. 14. (a) Hilbert transformed impulse response (average of 100 files) during the 2003 drift (time 23:00:00) and (b) blow-up of the main peak showing correlation amplitude with Hilbert envelope.

same shape. Again, despite its complexity the phase of the impulse response relative to the envelope can be distinguished.

In passing, it is interesting to note that the peak at 21 m (two-way path) in Fig. 14(a) is persistent throughout the 13 h drift and is believed to be a reflection from the weight at the bottom of the array. There is an equivalent peak in the 2004 measurements but at 24 m, probably because of minor differences in cable length. The fact that the same equipment and processing was used on the two occasions suggests that this is not a processing artifact but a true target detection using beam–beam cross correlation of noise.

Variation of peak amplitude with drift time is shown in Fig. 15. The mean is between about 0.021 and 0.015. The expected value according to Eq. (5) with $\gamma=12\,000/4166.7$, $\beta=1.87$ (bandwidth is half the design frequency), $z_2-z_1=110$ m is 0.0194, and again this agrees well with the experimental mean.

C. Ragusa Ridge 2004

These two drifts were a deliberate attempt to see how various noise inversion techniques would fare with a rough

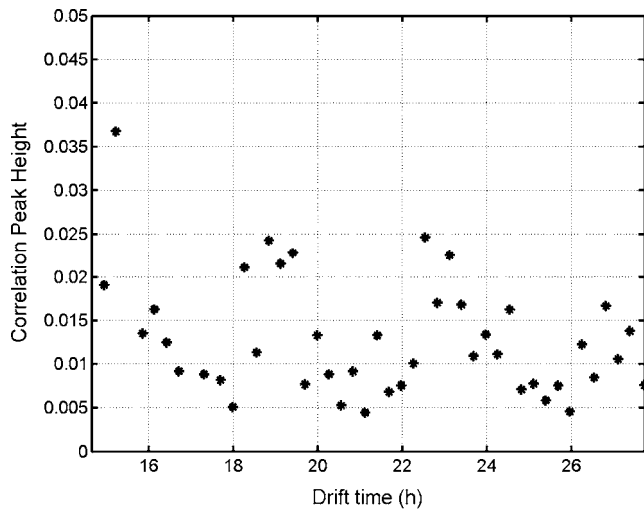


FIG. 15. Correlation peak amplitude (averaged over 100 files) vs drift time during the 2003 drift with the MFA.

seabed. A qualitative indication of the roughness is shown by the sidescan image in Fig. 16. The scales are known to be of order 1–10 m in the vertical and 10–20 m in the horizontal. Thus a coherent average along a drift track of, say 100 m, could be subject to very large vertical roughness excursions compared with those considered in Fig. 8.

From the point of view of cross-correlation techniques there were some additional potentially undesirable problems with acquisition and drop-outs, not to mention occasional nearby ships with singing propellers. On top of this, strong winds, which are usually ideal for generating sound, produced discrete, audible crashing waves. Nevertheless performance was distinctly better on the first day (12 May) than on the second (13 May). The reasons for this will become clear, and fortuitously provide some insight into the conditions under which a moving array can work.

1. Ragusa Ridge 2004 drift1

Figure 17(a) shows the profile obtained over 8 h. The blow-up in Fig. 17(b) emphasizes the variability in strength at the latter end of the drift and resembles an echo sounder record of a rough surface. The flatter sections in Fig. 17(a) between 20:00 and 21:00 and near 16:00 are thought to be

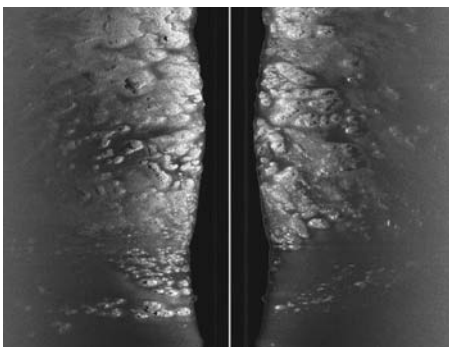


FIG. 16. Side-scan sonar image of part of the Ragusa Ridge showing features of 10–20 m in horizontal extent. Full cross-track range is 430 m.

small pools of sediment between rock outcrops, and one can see evidence of a weak second reflection a few meters later at both times.

There is a weakening of the echo in the central part of Fig. 17(a) which, from the considerations of Secs. II and III, cannot be caused by geographical changes in reflection coefficient, although they could be caused by changes in roughness. There were also no changes in instrumentation problems or weather conditions. The probable cause is suggested by the performance during the second drift (a day later).

2. Ragusa Ridge 2004 drift2

The 13 h second drift starting at almost the same location is shown in Fig. 18. The echo is so weak compared with the background that the contrast needed to be adjusted in order to see the bottom echo at all.

If anything, the instrumentation problems and weather conditions were less severe than during the first drift, but a clue as to the most likely cause of this varying performance is the relative lengths of the drift tracks (see Fig. 9) which were, after all, obtained for comparable durations. The average drift speed was just over twice as fast on the second day as on the first, as shown in Fig. 19.

The array's drift is driven by currents rather than wind since there is about 50 m of cable and array hanging vertically. In this area current variations of this magnitude from day to day are common (Lermusiaux and Robinson, 2001). As already discussed (Sec. II) the speed of the drift has little effect when the reflecting surface is flat since the Fermat travel time is independent of position, but when the surface is rough the Fermat path changes rapidly with position (and may be multivalued) so it may not be possible to average for long enough in each position for numerical convergence. The prime suspect for the weak echoes in this case is therefore the drift speed.

In retrospect the fade in the middle of Fig. 17(a) can also be attributed to variation in speed. Although the average speed for the 5 km was about 0.14 m/s there was some variation on 12 May as shown in Fig. 19. The rise in speed between 17:00 and 21:00 is closely matched by the fade. The smoother, flat bottomed section between 20:00 and 21:00 would be expected to survive by being more tolerant to high drift speed. In one sense this fading because of drift speed is a limitation of the technique when the surface is rough. In another sense it is a strength since the fading is unambiguously associated with drift speed and the fluctuations caused by a rough surface. As described here, this association is qualitative, but the effect is, in principle, quantifiable.

Although the reflecting surface is rough, steep angle returns appear not to be steep enough to register outside the rather broad endfire beam of this experimental arrangement. However the considerations of Sec. III suggest that, in principle, angle discrimination is possible given more amenable array designs.

V. CONCLUSIONS

The main point of this paper has been to understand the amplitude of the cross correlation between steered beams of

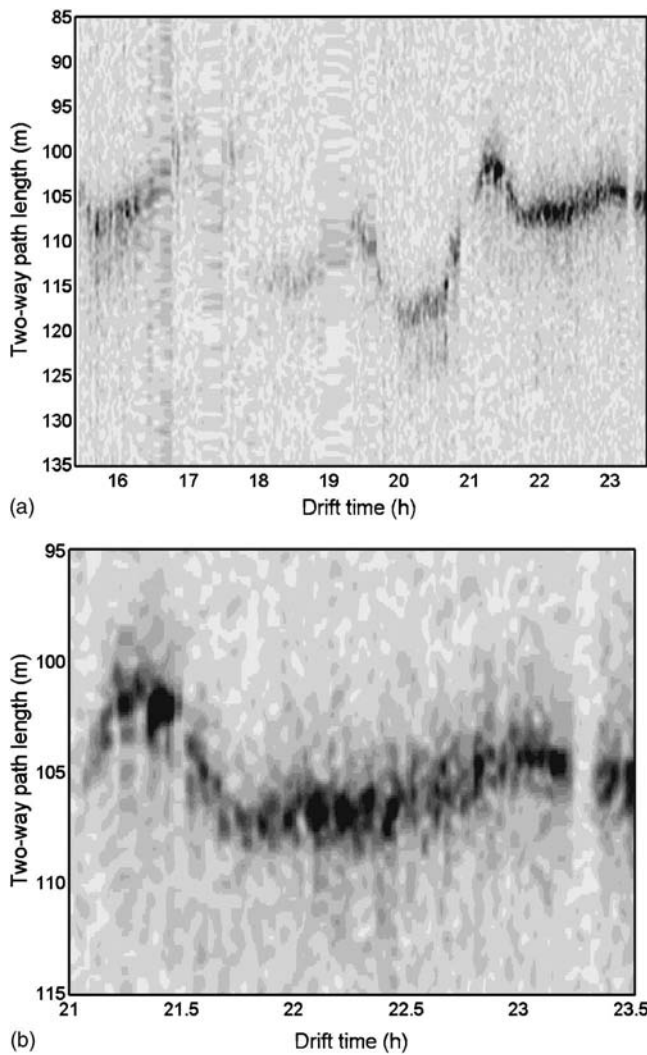


FIG. 17. Subbottom profile from the first MFA drift track on the Ragusa Ridge (2004) (a) showing fading bottom return during the centre portion and (b) a blow-up of the last 2 h.

ambient noise. The proposed normalization [Eq. (1)] results in a formula for peak height given by Eq. (5) which depends on the array size, the distance from the array to the reflector, the ratio of sample frequency to design frequency, but not the reflection coefficient, though relative strength of layers and their signs are retained, and there is sensitivity to the surface roughness through the reflection coherence.

A detailed theory is developed in the Appendix and summarized in Sec. II. This leads to a criterion for detecting a bottom echo in an uncorrelated background and an understanding of the effects of surface roughness, multiple layers, and tilted surfaces.

By representing the sheet of surface sources as many random time sequences emanating from random locations on a plane it was possible to simulate the direct and bottom reflected arrivals at the hydrophones of a vertical array. These were subsequently filtered, beam formed, and cross correlated using exactly the same algorithms as used for experimental data to confirm the theoretical predictions in all the earlier cases.

Finally experiments from three separate sea trials in the Mediterranean using two different arrays over smooth and

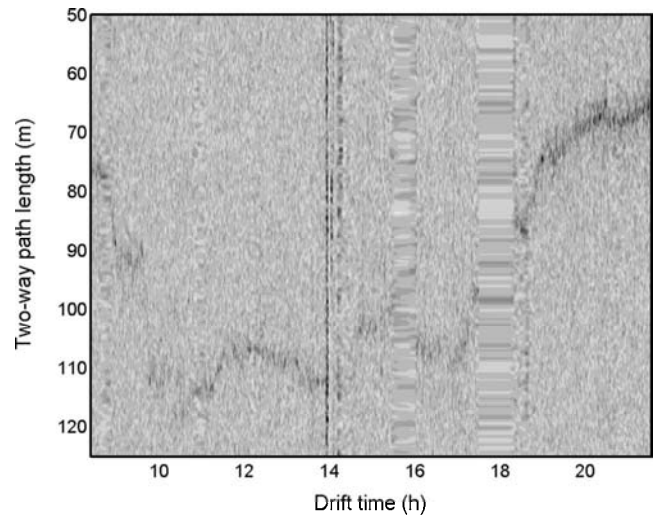


FIG. 18. Subbottom profile from the second MFA drift track on the Ragusa Ridge (2004) showing very weak bottom returns throughout.

rough seabed were processed to show bottom profiles and to investigate the correlation peak amplitudes versus drift time. By comparing the time differential of the beam-beam cross correlation with its Hilbert transform it was possible to distinguish phase changes between the layer reflections despite the rather oscillatory impulse response resulting from the prefiltering. The experimental amplitudes match the theoretical predictions well.

Obviously the correlation results are improved by longer integration times if the array and environment are stationary. When the bottom is smooth, horizontal motion of the array produces minimal effects, and therefore long integration times (coherent integration of many files) are feasible. When the bottom is rough, long integration times only enhance the echo if the array is motionless. The examples over the Ragusa Ridge exhibited large differences in drift speed during the two experiments that were clearly correlated with varia-

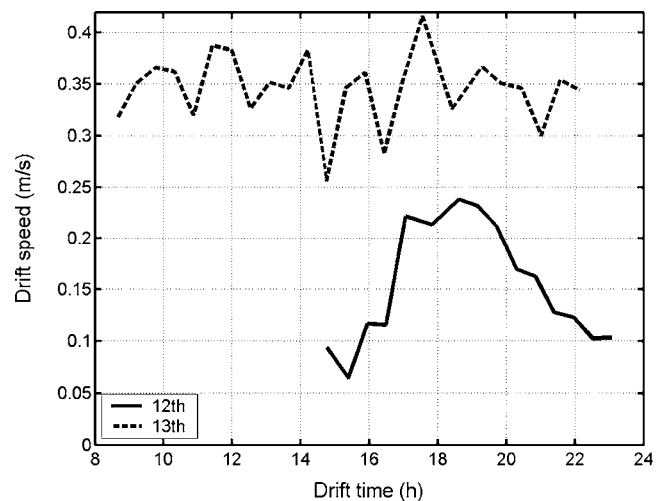


FIG. 19. Drift speed plotted against drift time for the two drifts over the Ragusa Ridge showing the marked difference and also the change during the first drift (12 May).

tion in echo strength. Thus a weak echo is a clear indication of a rough surface, regardless of the detailed motion or roughness dependence.

ACKNOWLEDGMENTS

The authors thank the Captain and crew of the *NRV Alliance*, Luigi Troiano and Enzo Michelozzi, for engineering coordination, Piero Boni for data acquisition, and particularly Peter Nielsen who acted as Scientist-in-charge during the three cited BOUNDARY experiments. They are also indebted to Roberto Rossi and Mark Prior for the side scan image.

APPENDIX: DERIVATION OF CROSS-CORRELATION PEAK AMPLITUDE

In this Appendix the numerator and denominator of the beam–beam cross correlation, Eq. (A1), are derived separately in terms of the source positions and physical delay times,

$$C(\tau) = \frac{\int g_1(t)g_2(t+\tau)dt}{\sqrt{\int g_1^2(t)dt \int g_2^2(t)dt}}. \quad (\text{A1})$$

The physics of the source wave form is deliberately simplified in order to separate out the effects due to delay time and “pure” randomness.

1. Definitions

At each randomly located source point n on the surface a time series $s_n(t)$ is emitted. This is uncorrelated with emissions from any other point m , i.e.,

$$\int s_n(t)s_m(t+\tau)dt = 0 \quad (\text{A2})$$

for $m \neq n$ and all τ greater than some limiting value τ_0 . In other words the time series though random may be spectrally “pink.” Taking the integral over a time T , $s_n(t)$ is related to its standard deviation through

$$\int s_n(t)s_n(t)dt = \sigma^2 T \quad (\text{A3})$$

and the normalized autocorrelation function of the individual sound sources is therefore given by

$$C_s(\tau) = \int s_n(t)s_n(t+\tau)dt / (\sigma^2 T). \quad (\text{A4})$$

The directional receiver at depth z in water of depth H has an upward beam and a downward beam. The downward beam is represented by its image in the seabed at depth H , i.e., an upward looking beam centered at depth $2H-z$. Thus the received amplitude for the generalized up/down beam $j=1, 2$ is

$$g_j(t) = \sum_n s_n(t-r_{jn}/c)b_{jn}R_{jn}/r_{jn}, \quad (\text{A5})$$

where r_{jn} , b_{jn} represent, respectively, the range and combined beam and source directionality factor associated with the j th beam and the n th noise source. The R_{jn} are generalized reflection coefficients. For the upward beam there is, of

course, no reflection and so $R_{1n}=1$.

2. Numerator

The numerator of Eq. (A1) is constructed from Eq. (A5) by making use of Eqs. (A2)–(A4) to get rid of the double sum and integral

$$\begin{aligned} & \int g_1(t)g_2(t+\tau)dt \\ &= \int \sum_m \sum_n s_n(t-r_{1n}/c)s_m(t-r_{2m}/c+\tau) \\ & \quad \times \frac{b_{1n}b_{2m}R_{1n}R_{2m}}{r_{1n}r_{2m}}dt \\ &= \int \sum_n s_n(t')s_n(t'+(\tau-\tau_r))\frac{b_{1n}b_{2n}R_{1n}R_{2n}}{r_{1n}r_{2n}}dt' \\ &= \sigma^2 T \sum_n C_s(\tau-\tau_r)\frac{b_{1n}b_{2n}R_{2n}}{r_{1n}r_{2n}}, \end{aligned} \quad (\text{A6})$$

where τ_r is the time difference between arrivals from the n th source and the two receivers, $\tau_r=(r_{2n}-r_{1n})/c$. Since these contributions only occur near the vertical the directionality factors can be replaced by the vertical beam power $b_{1n}^2=b_{2n}^2=b(0)$, and the vertical path lengths (z_1, z_2) substituted for (r_1, r_2). One can also assume that R_{2n} is the vertical reflection coefficient and drop the subscripts. To evaluate the sum each source point is assumed to occupy an elementary area A such that the sum can be written in terms of an integral over surface area,

$$\int g_1(t)g_2(t+\tau)dt = \frac{\sigma^2 T b(0)R(0)}{A z_1 z_2} \int_0^\infty C_s(\tau-\tau_r)2\pi\rho d\rho, \quad (\text{A7})$$

where ρ is a polar coordinate in the surface plane centered on the point above the receiver.

The travel time difference is related to the radius ρ by the Fresnel approximation

$$c\tau_r = r_{2n} - r_{1n} \cong z_2 - z_1 + \frac{\rho^2}{2} \left(\frac{1}{z_2} - \frac{1}{z_1} \right) \quad (\text{A8})$$

so

$$\rho d\rho = -cd\tau_r \frac{z_1 z_2}{z_2 - z_1}. \quad (\text{A9})$$

According to the above-mentioned Fresnel approximation a uniform distribution in area (i.e., $\rho d\rho$) results in a uniform distribution in time. It can be shown that, surprisingly, this is not true with exact Pythagoras path lengths although fortunately this is not important here.

Equation (A7) becomes

$$\int g_1(t)g_2(t+\tau)dt = -\frac{2\pi\sigma^2 T b(0)R(0)c}{A(z_2-z_1)} F(\tau) \quad (\text{A10})$$

$$F(\tau) = - \int_{\tau_z}^{\infty} C_s(\tau - \tau_r) d\tau_r = \int_{\tau - \tau_z}^{\infty} C_s(\tau') d\tau', \quad (\text{A11})$$

where $\tau_z = (z_2 - z_1)/c$ and the dummy variable is $\tau' = \tau - \tau_r$. If the noise sources had a true uniform spectrum then C_s would be a Kronecker delta function, and so the integral would be unity for $\tau < \tau_z$ and zero for $\tau > \tau_z$, i.e., a step function. To obtain the Green's function as in, for example, Eqs. (1) and (2) of Roux *et al.* (2005), one needs to differentiate Eq. (A10) with respect to τ , in which case F itself becomes a Kronecker delta,

$$\frac{\partial}{\partial \tau} \int g_1(t) g_2(t + \tau) dt = \frac{2\pi\sigma^2 T b(0) R(0) c}{A (z_2 - z_1)} C_s(\tau). \quad (\text{A12})$$

Numerically this can be found from the forward difference (indicated by Δ) of the correlation divided by the sample interval. In the (continuous) frequency domain it is equivalent to multiplication by frequency. The Discrete Fourier Transform (DFT) equivalent of differentiation is convolution by two opposite signed Kronecker delta functions separated by one sample (interval T_s), which is equivalent to multiplication by $(1 - \exp(-i2\pi f T_s))$ in the frequency domain followed by division by T_s . Thus numerically one would find

$$\Delta \left\{ \int g_1(t) g_2(t + \tau) dt \right\} = \frac{2\pi\sigma^2 T b(0) R(0) c}{A f_s (z_2 - z_1)} C_s(\tau) \quad (\text{A13})$$

and the peak value would be

$$\max \left[\Delta \left\{ \int g_1(t) g_2(t + \tau) dt \right\} \right] = \frac{2\pi\sigma^2 T b(0) R(0) c}{A f_s (z_2 - z_1)}. \quad (\text{A14})$$

Because R retains its sign, the term ‘‘max’’ is used here to mean the maximum of the absolute value multiplied by the sign.

Otherwise if one retains the original spectrum, $\bar{s}(\omega) = \int_{-\infty}^{\infty} s(\omega) \exp(-i\omega t) d\omega$, but sets the near zero frequencies to zero, $|\bar{s}(0)|^2 = 0$, then an identity that follows from the Wiener-Khinchine theorem (p.141, Skudrzyk, 1971) states that

$$\int_{-\infty}^{\infty} C_s(\tau') d\tau' \equiv |\bar{s}(0)|^2 = 0. \quad (\text{A15})$$

The function F in Eq. (A10) is therefore still zero for large positive or negative $\tau - \tau_z$. Where $\tau \sim \tau_z$ the function may oscillate, but the absolute value of its Hilbert transform, being the envelope of the oscillation, provides a good representation, though slightly widened, of the Kronecker delta. The penalty is loss of the sign of the impulse response.

Thus there are two processing options, one is to opt for robustness and retain the Hilbert transform (with or without the time differentiation). The other is to perform the differentiation without Hilbert transform and thus retain a signed impulse response.

This time domain derivation has essentially assumed a broad band. If the spectrum of the source term is assumed to be flat (σ^2 is the source variance for the given band), then narrowing its band (by filtering) reduces the height of the

correlation peak (through σ^2) and therefore the amplitude response [Eqs. (A10) and (A11)] in proportion to the band, and the power response in proportion to bandwidth squared (as can easily be seen by consideration of a Gaussian spectral shape and its corresponding Gaussian autocorrelation function).

3. Denominator

The amplitude of the numerator of Eq. (A1) is not much use alone since it contains the unknowns σ , T , A . The normalization, i.e., the denominator of Eq. (A1), resolves this because it is proportional to the same unknowns. Each of the two components of the denominator of Eq. (A1) is evaluated as

$$\begin{aligned} \int g_j^2(t) dt &= \int \sum_m \sum_n s_n(t - r_{jn}/c) s_m(t - r_{jm}/c) \\ &\quad \times \frac{b_{jn} b_{jm} R_{jn} R_{jm}}{r_{jn} r_{jm}} dt \\ &= \sigma^2 T \sum_n \frac{b_{jn}^2 R_{jn}^2}{r_{jn}^2}, \end{aligned} \quad (\text{A16})$$

where use has been made of Eqs. (A2) and (A3) to reduce the integral and double sum to a single sum. To evaluate the sum each source point is again assumed to occupy an elementary area A such that the sum can be written in terms of an integral over surface area. So now

$$\int g_j^2(t) dt = \frac{2\pi\sigma^2 T}{A} \int_0^{\infty} \frac{b_j^2 R_j^2}{r_j^2} \rho d\rho, \quad (\text{A17})$$

where ρ is the polar coordinate in the surface plane centered on the point above the receiver. Notice that in Eq. (A17) the reflection coefficient is squared so that its sign is lost, in contrast with behavior in Eq. (A14). The area integral can be transformed into an angle integral (which does not depend on the distance of the receiver from the surface)

$$\int_0^{\infty} \frac{b_j^2}{r_j^2} \rho d\rho = b(0) \int_0^{\pi/2} B(\theta) N(\theta) \cos \theta d\theta \quad (\text{A18})$$

and this is recognized as the integral that appears in the array gain (or noise gain) formula (Urlick, 1975), where N is the noise directionality [so that the complete noise source term is $\sigma^2 N(\theta)$] and B is the array's beam pattern, normalized to unity in the steer direction. It can be evaluated straightforwardly by expressing it as the sum of the terms in the noise's normalized cross-spectral density matrix C_{ij} weighted by the array shading w_i and with steering phases ϕ_{ij} (Urlick, 1975),

$$\begin{aligned} \int_0^{\pi/2} B(\theta) N(\theta) \cos \theta d\theta &= \frac{\sum_{i,j}^{MM} \{w_i w_j C_{ij} \exp(i\phi_{ij})\}}{\left(\sum_i^M w_i \right)^2} \\ &\quad \times \int_0^{\pi/2} N(\theta) \cos \theta d\theta \end{aligned} \quad (\text{A19})$$

If it is assumed that the surface noise sources have a dipole

directionality then, since $N = \sin \theta$, the noise integral is $\int_0^{\pi/2} N(\theta) \cos \theta d\theta = 1/2$, and the normalized C_{ij} are (Cron and Sherman, 1962; 1965)

$$C_{ij} = C(kd_{ij}) = 2\{\exp(ikd_{ij})/(ikd_{ij}) + (\exp(ikd_{ij}) - 1)/(kd_{ij})^2\}. \quad (\text{A20})$$

Assuming hamming shading the integral of Eq. (A19) is just a number,

$$\beta \equiv M \frac{\sum_{i,j}^{MM} \{w_i w_j C_{ij} \exp(i\phi_{ij})\}}{2 \left(\sum_i^M w_i \right)^2}, \quad (\text{A21})$$

where M is the number of hydrophones. This result can be inserted directly into Eq. (A17) for $j=1$, but for $j=2$, it is noted that the Rayleigh reflection coefficient is a function of vertical wave number, which is necessarily slowly varying near vertical, so it will be assumed that it remains constant over the endfire beam. It can therefore be taken out of the integral and the same noise gain integral is obtained for both beams.

The final result is

$$\sqrt{\int g_1^2(t) dt \int g_2^2(t) dt} = \frac{2\pi\sigma^2 T b(0) |R(0)| \beta}{A M}. \quad (\text{A22})$$

Assuming the spectrum of the source term to be flat, as in the second section of the Appendix (σ^2 is the source variance for the given band), a narrowing of the band (by filtering) reduces the response in proportion, again through σ^2 . An additional effect is due to the dependence of beam width on frequency (in fact, inverse proportionality). This controls the numerical value of β , [Eq. (A21)]. For a narrow band at the design frequency $\beta=1.38$; for a band extending from the design frequency down to half the design frequency it is $\beta=1.87$; for a band extending down to almost zero (design frequency/200) it is $\beta=4.08$. This additional effect is therefore merely an averaging over frequency.

4. Complete formula for peak value

Combining Eqs. (A10) and (A22) to form Eq. (A1) gives

$$\max[\Delta\{C(\tau)\}] = \frac{cM \text{sign}(R)}{(z_2 - z_1) f_s \beta} \quad (\text{A23})$$

As explained earlier the main bandwidth effects have canceled out leaving the minor effect of frequency averaging the beam width incorporated in β . Since the hydrophone separation a and the design frequency are related by $2f_0 a = c$ Eq. (A23) can be written in terms of the array's acoustic length ($L = Ma$) as

$$\max[\Delta\{C(\tau)\}] = \frac{2f_0 L \text{sign}(R)}{(z_2 - z_1) f_s \beta}. \quad (\text{A24})$$

The ratio of sample frequency to design frequency is also a number $\gamma = f_s / f_0$ so the final peak value is

$$\max[\Delta\{C(\tau)\}] = \frac{2L \text{sign}(R)}{(z_2 - z_1) \gamma \beta}. \quad (\text{A25})$$

For the equipment used here there are 32 hydrophones separated by 0.18 m with a design frequency of 4166.7 Hz and a sampling frequency of 12 kHz. A height above the seabed of 30 m leads to $z_2 - z_1 = 60$ m, and assuming the band is half the design frequency ($\beta = 1.87$), the final peak height is 0.0357. Alternatively, assuming the band to be the full design frequency ($\beta = 4.08$), the final peak height is 0.0164.

5. Complete formula for background

Away from the peak cross correlation with a finite number N of samples the background will not be exactly zero as implied by Eqs. (A6) and (A1). In a loose sense it is related to the number of independent samples; more exactly the background [i.e., the standard deviation of Eq. (A1)] is derived as follows. Each background sample ν_m [i.e., realization of C in Eq. (A1)] is the sum of the product of two (potentially correlated) sequences $b_m = \sum_n^N f_{n,m}$, where $f_{n,m} = p_n q_{n+m}$. Although the probability distribution of the product is not Gaussian it can be shown that the variance of the product is the product of the individual variances, say σ^2 . The variance of the background is the mean of the squares of these sums, i.e.,

$$\begin{aligned} m\sigma_b^2 &= \sum_m \left(\sum_n^N (f_{n,m}) \right)^2 = \sum_m \sum_n^N \sum_{n'}^N f_{n,m} f_{n',m} \\ &= \sigma^2 \sum_m \sum_n^N \sum_{n'}^N \rho_{(n-n'),m}. \end{aligned} \quad (\text{A26})$$

The last double sum is the sum over the correlation coefficients ρ which for large N leads to $\sigma_b^2 = N\sigma^2 \sum_{j=-N}^N \rho_j$. Since the peak value is $N^2\sigma^2$ the normalized background variance is $\sum_{j=-N}^N \rho_j / N$ which can be thought of as the reciprocal of the number of independent samples in f .

Brekhovskikh, L., and Lysanov, Yu., (1982). *Fundamentals of Ocean Acoustics* (Springer, New York).

Buckingham, M. J., and Jones, S. A. S., (1987). "A new shallow-ocean technique for determining the critical angle of the seabed from the vertical directionality of the ambient noise in the water column," *J. Acoust. Soc. Am.* **81**, 938–946.

Cato, D. H., (2000). "Sea-surface generated noise dependence on wind speed and white cap coverage," *J. Acoust. Soc. Am.* (A) **107**, 2922.

Cron, B. F., and Sherman, C. H., (1962). "Spatial correlation functions for various noise models," *J. Acoust. Soc. Am.* **34**, 1732–1736.

Cron, B. F., and Sherman, C. H., (1965). "Addendum: Spatial correlation functions for various noise models [*J. Acoust. Soc. Am.* 34, 1732–1736 (1962)]," *J. Acoust. Soc. Am.* **38**, 885.

Ding, L., and Farmer, D. M., (1994). "Observations of breaking surface wave statistics," *J. Phys. Oceanogr.* **24**, 1368–1387.

Finette, S., and Heitmeyer, R. M., (1996). "Angle-time-frequency resolution of the noise field generated by wind-induced breaking waves," *J. Acoust. Soc. Am.* **99**, 209–222.

Frison, T. W., Abarbanel, H. D. I., Cembrola, J., and Neales, B., (1996). "Chaos in ocean ambient 'noise'," *J. Acoust. Soc. Am.* **99**, 1527–1539.

Harrison, C. H., (1996). "Formulas for ambient noise level and coherence," *J. Acoust. Soc. Am.* **99**, 2055–2066.

Harrison, C. H., (2004). "Sub-bottom profiling using ocean ambient noise," *J. Acoust. Soc. Am.* **115**, 1505–1515.

Harrison, C. H., (2005). "Performance and limitations of spectral factorization for ambient noise sub-bottom profiling," *J. Acoust. Soc. Am.* **118**,

- 2913–2923.
- Harrison, C. H., and Simons, D. G., (2002). “Geoacoustic inversion of ambient noise: a simple method,” *J. Acoust. Soc. Am.* **112**, 1377–1389.
- Lermusiaux, P. F. J., and Robinson, A. R., (2001). “Features of dominant mesoscale variability, circulation patterns and dynamics in the Strait of Sicily,” *Deep-Sea Research, Part I* **48**, 1953–1997.
- Melville, W. K., and Matusov, P., (2002). “Distribution of breaking waves at the ocean surface,” *Nature (London)* **417**, 58–63.
- Roux, P., and Kuperman, W. A., (2004). “Extracting coherent wave fronts from acoustic ambient noise in the ocean,” *J. Acoust. Soc. Am.* **116**, 1995–2003.
- Roux, P., Sabra, K. G., Kuperman, W. A., and Roux, A., (2005). “Ambient noise cross correlation in free space: Theoretical approach,” *J. Acoust. Soc. Am.* **117**, 79–84.
- Sabra, K. G., Roux, P., and Kuperman, W. A., (2005). “Emergence rate of the time-domain Green’s function from the ambient noise cross-correlation function,” *J. Acoust. Soc. Am.* **118**, 3524–3531.
- Sabra, K. G., Roux, P., Kuperman, W. A., Hodgkiss, W. S., and D’Spain, G. L., (2004). “Using ocean ambient noise for array element localization,” *J. Acoust. Soc. Am. (A)* **115**, 2507.
- Siderius, M., Harrison, C. H., and Porter, M. B., (2006). “A passive fathometer technique for imaging seabed layering using ambient noise,” *J. Acoust. Soc. Am.* **120**, 1315–1323.
- Skudrzyk, E., (1971). *The Foundations of Acoustics*, (Springer, New York).
- Urick, R. J., (1975). *Principles of Underwater Sound*, 2nd ed. (McGraw-Hill New York), Chap. 7.
- Weaver, R. L., and Lobkis, O. I., (2004). “Diffuse fields in open systems and the emergence of the Green’s function,” *J. Acoust. Soc. Am.* **116**, 2731–2734.

Document Data Sheet

<i>Security Classification</i> NATO UNCLASSIFIED		<i>Project No.</i>
<i>Document Serial No.</i> NURC-PR-2008-004	<i>Date of Issue</i> September 2008	<i>Total Pages</i> 15 pp.
<i>Author(s)</i> Harrison, C.H., Siderius, M.		
<i>Title</i> Bottom profiling by correlating beam-steered noise sequences		
<i>Abstract</i>		
<i>Keywords</i>		
<i>Issuing Organization</i> NURC Viale San Bartolomeo 400, 19126 La Spezia, Italy [From N. America: NURC (New York) APO AE 09613-5000]		Tel: +39 0187 527 361 Fax: +39 0187 527 700 E-mail: library@nurc.nato.int